

## DERIVATION OF FOREST LEAF AREA INDEX FROM MULTI- AND HYPERSPECTRAL REMOTE SENSING DATA

*Martin Schlerf, Clement Atzberger, Michael Vohland, Henning Buddenbaum,  
Stephan Seeling and Joachim Hill*

Trier University, Department of Remote Sensing, D-54286 Trier, Germany;  
[schlerf\(at\)uni-trier.de](mailto:schlerf(at)uni-trier.de)

### ABSTRACT

This study evaluated systematically linear predictive models between vegetation indices (*VIs*) derived from radiometrically corrected airborne imaging spectrometer (HyMap) data and field measurements of leaf area index (*LAI*) ( $n=40$ ). Ratio-based and soil-line related broadband *VIs* were calculated after HyMap reflectance had been spectrally resampled to Landsat TM channels. Hyperspectral *VIs* involved all possible types of 2-band combinations of *RVI* and *PVI*. Cross-validation procedure was used to assess the prediction power of the regression models. Analyses were performed on the entire data set or on subsets stratified according to stand age. A perpendicular vegetation index (*PVI*) based on wavebands at 1,088 and 1,148 nm was linearly related to leaf area index (*LAI*) ( $R^2=0.67$ ,  $RMSE=0.69 \text{ m}^2\text{m}^{-2}$  (21% of the mean); after removal of one forest stand subjected to clearing measures:  $R^2=0.77$ ,  $RMSE=0.54 \text{ m}^2\text{m}^{-2}$  (17% of the mean)). The study demonstrates that for hyperspectral image data, linear regression models can be applied to quantify *LAI* with good accuracy. Best hyperspectral *VIs* in relation with *LAI* are typically based on wavebands related to prominent water absorption features. Such *VIs* measure the total amount of canopy water; as the leaf water content is considered to be relatively constant in the study area, variations of *LAI* are retrieved.

**Keywords:** Hyperspectral, vegetation indices, forest, leaf area index

### INTRODUCTION

The majority of studies for extracting biophysical variables from remotely sensed data have used empirical techniques to relate the spectral measurements to biophysical parameters (1). While much work has been done with agricultural crops, relatively little research has been done on investigating the relationships between forest leaf area index (*LAI*) and satellite data (2). Most of the studies on forests have used broadband *VIs* (e.g. *NDVI*, *RVI*) to derive *LAI* of coniferous forest stands; however, with varying success (3;4,5,6,7,8;9). Few studies looked at the suitability of high spectral resolution remote sensing data to derive the *LAI* of coniferous forests. (10) tested CASI data using univariate and multivariate regression and a *VI* based algorithm and found strong relationships with reasonable low errors. (11) tested if the red edge inflection point (*REIP*) is primarily controlled by forest canopy *LAI* using helicopter-borne spectroradiometer data and found a strong non-linear correlation between plot *LAI* and the *REIP* for Sitka spruce (*Picea sitchensis*). For the same tree species, forest *LAI* was recently related to the canopy *REIP* computed from imaging spectrometer data (CASI) with success (12). Despite the research undertaken it is often unclear whether the high spectral resolution data offer advantages over broadband data (13).

The overall aim of the work was to evaluate the information content of hyperspectral remote sensing data for the estimation of forest *LAI* in comparison with broadband data. More specific objectives were (i) to determine spectral vegetation indices (*VI*) that are best suited for characterising *LAI*, and (ii) to compare and contrast traditional broad-band and hyperspectral *VIs* in terms of basic statistical characteristics of the predicted relative to the observed *LAI*. The research was restricted to Norway spruce as only forest stands of this single species occur in sufficient numbers within the selected test site. Besides, coniferous forests do not show a saturation of *VI* with in-

creasing *LAI*, whereas the saturation effect limits the usefulness of optical remote sensing for biophysical parameter mapping for mature deciduous forests (9).

## MATERIAL AND METHODS

The Idarwald forest (49°45'N, 7°10'E) is located on the north-western slopes of the Hunsrück mountain ridge, Germany. It covers an area of about 7,500 ha. In 1999, 42 relatively homogenous Norway spruce (*Picea abies*) stands were identified at the Idarwald study area. Within these stands, 42 square 0.09 ha plots were established. The central location of each ground plot was determined with an accuracy of about  $\pm 5$  m using a differential global positioning system (GPS). Signal distortion within the forest stands did not give as high accuracies as specified by the manufacturer. Of a total of 42 stands, one was not covered by the HyMap imagery, and another one was thinned in the period between ground data collection and the HyMap overpass. These two stands were excluded from the analysis reducing the data set to 40 stands.

At each plot, measurements of forest leaf area index (*LAI*) were carried out. *LAI* was estimated using a Li-Cor LAI-2000 instrument. The instrument was only operated under overcast sky conditions. Within each plot, Li-Cor measurements were taken at ten regularly spaced points from which the average was calculated. Above the canopy measurements were taken in a nearby open field before entering the plots. Although Li-CoR measurements represent rather an effective plant area index instead of the real leaf area index due to the non-random distribution of leaves, no corrections were applied.

To improve *LAI* mapping it has been suggested to derive land cover specific *VI-LAI* relationships using land cover maps (7,9). This stratification process is usually based on the species type. As in the present study just one single species is considered, it was decided to stratify the data set according to stand age (Table 1).

Table 1: Resulting subsets after stratification according to forest stand age

Subset	Designation	Abbreviation	Age	n
1	total (pooled dataset)	t	10-148	40
2	medium to old	mo	30-148	35
3	old	o	80-148	17
4	medium	m	30-79	18
5	young	y	10-29	5

The hyperspectral HyMap sensor (Integrated Spectronics, Australia) was flown over the Idarwald test site on 17 July 1999. The data were recorded at 13:00 hrs CET at an average flying height of 1,980 m above ground level and free of cloud cover. The resulting ground resolution was about 5 m with a full scene covering approximately 3 km x 10 km. From the original data cube with 128 bands between 400 and 2,500 nm, 14 HyMap spectral channels with high noise were identified as bad bands and removed from the data set. Consequently, subsequent analyses were restricted to the remaining 114 bands. To correct the view angle effect, an across track illumination correction was applied to each spectral band independently (ENVI 3.4, Research Systems). For this purpose, a second-order polynomial was fitted to the data. Based on the fitted polynomials, a normalization procedure was applied. The radiometric correction steps applied to the HyMap data consisted of the atmospheric correction, the correction for illumination effects caused by topography, and the in-flight calibration of the HyMap sensor system (14). The image data were geometrically corrected using the parametric geocoding software PARGE (15). For this purpose, the required DEM with an original pixel size of 20 m was resampled to 5 m. Mean reflectance spectra were extracted from the image data at a fixed radius around the central position of each test plot (GPS measurement).

Table 2: Broadband and hyperspectral vegetation indices investigated in this study.  
 $\rho$ =reflectance, TM=Thematic Mapper

Name	Abbreviation	Equation	Reference
Ratio vegetation index	<i>RVI</i>	$RVI = \frac{\rho_{TM4}}{\rho_{TM3}}$	(16)
Normalised difference vegetation index	<i>NDVI</i>	$NDVI = \frac{\rho_{TM4} - \rho_{TM3}}{\rho_{TM4} + \rho_{TM3}}$	(17)
Perpendicular vegetation index	<i>PVI</i>	$PVI = \frac{\rho_{TM4} - a\rho_{TM3} - b}{\sqrt{1 + a^2}}$ $a = 0.9, b = 0.1$	(18)
Transformed soil-adjusted vegetation index	<i>TSAVI</i>	$TSAVI = \frac{a(\rho_{TM4} - a\rho_{TM3} - b)}{a\rho_{TM4} + \rho_{TM3} - ab}$ $a = 0.9, b = 0.1$	(19)
Mid-infrared vegetation index	<i>MVI</i>	$MVI = \frac{\rho_{TM4}}{\rho_{TM5}}$	(2)
Greenness vegetation index	<i>GVI</i>	$GVI = -0.2848\rho_{TM1} - 0.2435\rho_{TM2} - 0.5436\rho_{TM3} + 0.7243\rho_{TM4} + 0.0840\rho_{TM5} - 0.1800\rho_{TM7}$	(20)
Narrowband RVI	$RVI_{Bd1,Bd2}$	$RVI_{Bd1,Bd2} = \frac{\rho_{Bd1}}{\rho_{Bd2}}$	(21)
Narrowband PVI	$PVI_{Bd1,Bd2}$	$PVI_{Bd1,Bd2} = \frac{\rho_{Bd1} - a\rho_{Bd2} - b}{\sqrt{1 + a^2}}$	

Both hyperspectral and broadband VIs were computed from the radiometrically corrected HyMap imagery (Table 2). Ratio-based and orthogonal broadband VIs were calculated after the HyMap data had been resampled to Landsat TM spectral bands involving the appropriate Landsat TM 5 filter functions; the ratio-based VIs were *RVI* and *NDVI*; the orthogonal VIs were *PVI* and *TSAVI*; additional VIs were *MVI*, and *GVI*. Hyperspectral (narrowband) indices were computed for *RVI* and *PVI* involving all possible two-band combinations of 114 channels (12,996 band combinations). *PVI* requires site-specific soil line slopes *a* and intercepts *b*. As no soil spectral data was available, standard values ( $a=0.9$ ;  $b=0.1$ ) were used. It was assumed that the soil line concept, originally defined for the red-nIR feature space, can be transferred into other spectral domains (21). Hence, it was supposed that soil lines exist between all wavebands.

Linear regression was employed to evaluate the relationships between biophysical stand variables and *VI*. For conifers it has been shown, that linear regression models seem to be appropriate as saturation occurs only at relatively high densities (6,9). The cross-validation procedure was used to validate the regression models. The cross-validated *RMSE* is a good indicator of the accuracy of the model in predicting unknown samples.

## RESULTS AND DISCUSSION

Although forest stands from very young to very old stands were probed, the variation of *LAI* values is rather moderate (Table 3). *LAI* was most strongly correlated with TM4, less correlated with TM3, and least correlated with TM5 (Table 4). Correlations in all bands were positive. Correlation spectra were computed for reflectance and first derivative of reflectance (not shown). The strength of the relations with *LAI* generally decreases from nIR to mIR wavebands and is greater for first derivative reflectance spectra in opposition to reflectance spectra. The nIR region of reflectance

spectra reveals the highest correlations followed by the green peak, the mIR region, and the chlorophyll absorption features in the red and blue wavebands.

Table 3: Summary statistics of forest stand variables (n=40)

	Mean	Standard deviation	Maximum	Minimum	Range
LAI /m <sup>2</sup> m <sup>-2</sup>	3.24	0.97	5.47	1.66	3.81

Table 4: Linear correlation between forest LAI and HyMap reflectance resampled to TM spectral bands (n=40); \*\* correlation coefficient significant at P<0.01, \* correlation coefficient significant at P<0.05

	TM3	TM4	TM5
LAI	0.36*	0.76**	0.33*

An inverse relationship can be observed in Figure 1, where LAI is plotted against stand age for the probed Norway spruce stands of Idarwald test site. The inverse relation between LAI and stand age seems to be related to the fact that during stand development, crowns of individual trees expand and increase utilization of available growing space. The point at which crowns of different trees begin to interact is considered as being the peak LAI after which a rapid decrease takes place due to competition between the individual trees (22). It has been shown that stands of slowly growing species (*pinus contora*) reached its maximum LAI at age 40 and that it lasted for about 30 years (22). In Figure 1, a peak LAI can be assumed at an age of 20. From an age of 20 onwards, a gradual decline in LAI up to age 150 is evident. Maximum variation of LAI occurs at age 60-70. Obviously, some stands have been thinned lately whereas others have been thinned a long time ago. After an increase of LAI up to age 100 a decrease of LAI is caused by gaps related to logging measures. It can be concluded that the observed age course of Norway spruce based on the probed sample is a result of both natural circumstances and actual management practices. It is also clear from Figure 1, that LAI can vary considerably within a single age class and thus, information on LAI cannot simply be derived from an age class map.

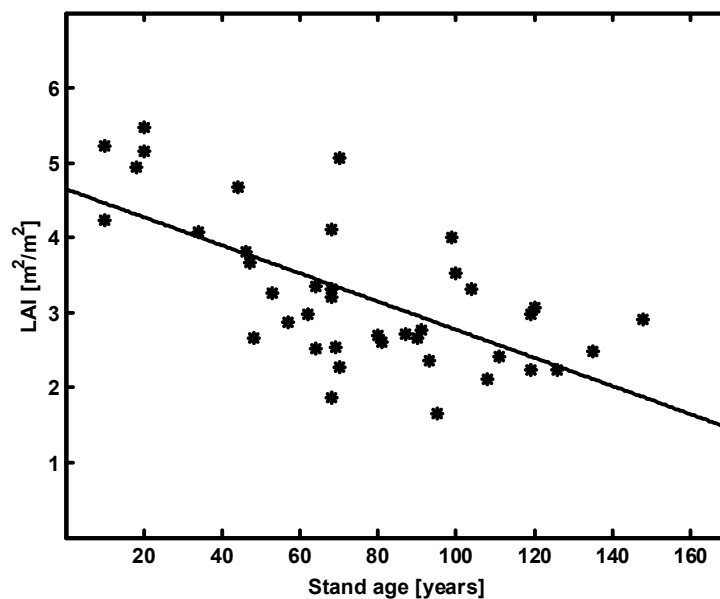


Figure 1: LAI as a function of stand age for Norway spruce stands at Idarwald test site (n=40).

To determine optimal narrowband VIs, coefficients of determination ( $R^2$ ) between all possible two-band VIs and LAI were computed. The results are illustrated in 2D-correlation plots (Figure 2). Based on the  $R^2$  values in the 2D-correlation plots, band combinations that form the best indices

were determined. These were considered as optimal indices and were named *RVI<sub>opt</sub>* and *PVI<sub>opt</sub>*. Up to three best performing indices were considered when they occurred in different wavelength regions. For example, in Figure 2, the indices that have highest correlation with *LAI* were extracted from the 2D-correlation plot range above 0.80; the three most dominant indices occur in the regions around 1,346nm/1,207nm, 1,134nm/920nm, and 1,802nm/1,163nm. The band positions were then tabulated in Table 5. For the best performing narrowband index, cross-validated *R<sup>2</sup>* and *RMSE* were computed (Table 6).

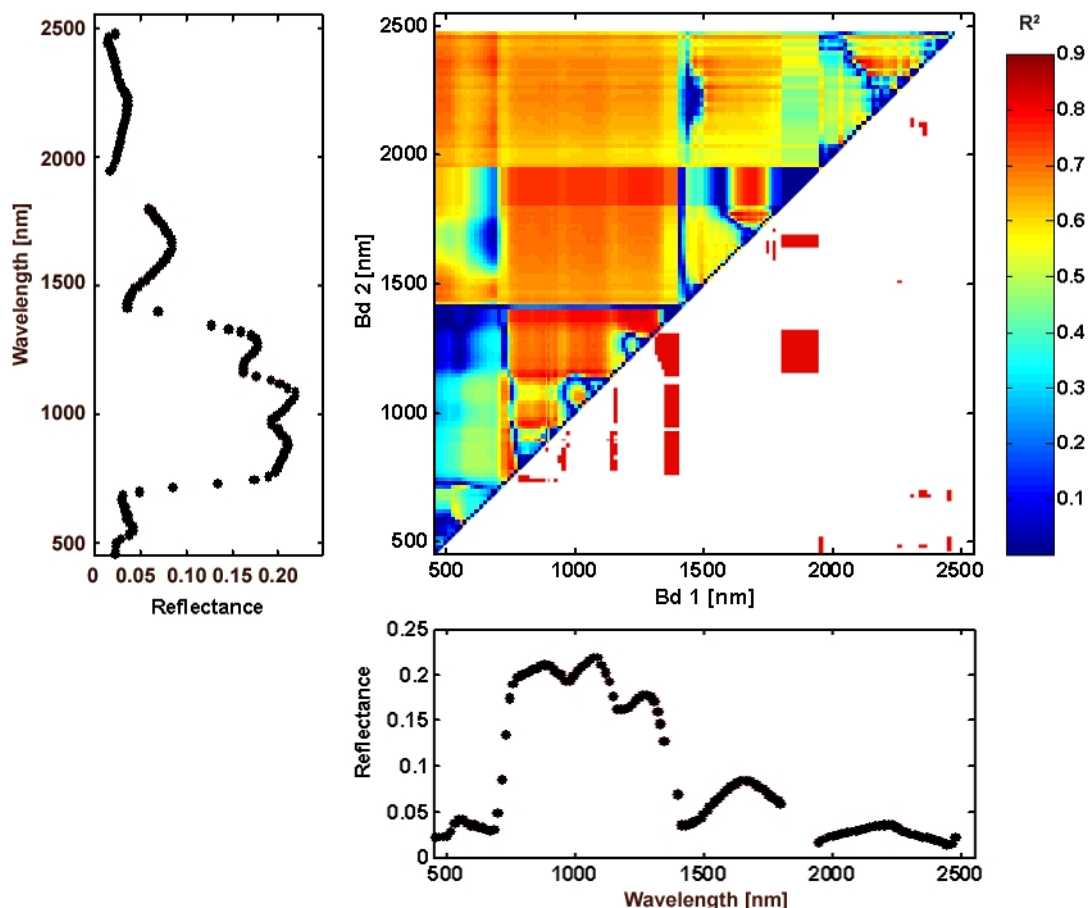


Figure 2: 2D-correlation plot that shows the correlation ( $R^2$ ) between LAI and narrowband RVI values (subset *m*). The matrix is symmetrical, therefore just values above the diagonal are displayed. Below the diagonal, band combinations are marked in red where  $R^2 > 0.75$ . The displayed average reflectance spectrum of all measured forest plots facilitates the interpretation of the 2D-correlation plot.

Table 5: Best narrowband RVI and PVI derived from 2D-correlation plots for different subsets. Subset *y* was excluded from the analysis due to the small number of samples

	t (10-148 years)		mo (30-148 years)		o (80-148 years)		m (30-79 years)	
	$\lambda$ /nm	$r^2$	$\lambda$ /nm	$r^2$	$\lambda$ /nm	$r^2$	$\lambda$ /nm	$r^2$
<i>RVI<sub>opt</sub></i>	918/965	.65	896/965	.68			1346/1207	.85
	850/680	.55	1802/1043	.65	747/807	.60	1134/920	.85
	1165/750	.60	1346/1119	.65			1802/1163	.80
<i>PVI<sub>opt</sub></i>	1088/1148	.70					918/1134	.83
	1148/807	.70	895/1134	.64	1445/2060	.56	1320/1220	.82
							2220/457	.72

Table 6: Cross-validated  $R^2$  (first line) and cross-validated RMSE (second line) for linear regression between broadband and hyperspectral vegetation indices and forest stand LAI. The best VIs are typed in bold. Subset *y* was excluded from the analysis due to the small number of samples

	Subset	t	mo	m	o
	<i>n</i>	40	35	17	18
Broadband VI	<i>RVI</i>	.40	.42	.40	.17
		1.23	.92	1.05	1.67
	<i>NDVI</i>	.43	.44	.44	.17
		1.13	.86	.95	1.72
	<i>PVI</i>	.57	.29	.23	.22
		.87	1.29	1.7	1.7
	<i>TSAVI</i>	.61	.36	.30	.24
		.80	1.06	1.35	1.55
	<i>MVI</i>	.38	.54	.58	.35
		1.3	.71	.71	1.83
	<i>GVI</i>	.58	.31	.24	.24
		.85	1.2	1.62	1.55
Hyper-spectral VI	<i>RVI_opt</i>	.62	.64	.77	.57
		.78	.58	.45	.57
	<i>PVI_opt</i>	.67	.45	.41	.52
		.69	.86	1.02	.58

The first step in the analysis of broadband VIs was to compare ratio to soil-adjusted VIs and to compare VIs based on Vis and nIR reflectance to those based on mIR and nIR reflectance. Broadband ratio VIs (*RVI* and *NDVI*) generally show relatively low values of  $R^2$  and relatively high values of RMSE for all subsets. The soil-adjusted broadband models (*PVI* and *TSAVI*) perform significantly better for the pooled data set; obviously, background effects related to soil and litter were reduced. While younger stands reveal a denser canopy with little background contribution to the signal, the background may have a larger influence on reflectance in older stands with gaps and a more open canopy. Hence, when the total age dynamic is considered, *TSAVI* and *PVI* perform better than *RVI* or *NDVI*, but when age classes are considered separately no performance increase is observed. The findings of (8), that soil-adjusted VIs compared to the *RVI* have a decreased sensitivity to forest *LAI*, can not be confirmed.

Broadband *MVI* is more closely related to *LAI* than broadband *RVI* and *NDVI* (subset *m* and *mo*). The mIR band in combination with the nIR band seems to contain more information relevant to the characterisation of forest canopies than the combination of red and nIR bands. Recently, a closer relation of forest *LAI* to radiation in the mIR than to radiation in the VIs was found by (23) for tropical vegetation; the authors put forward that this could be the case also with boreal forests. The results found in the present study also support the suggestion by (2) that mIR bands may improve *LAI* estimation, particularly in more open forest stands.

In the second step of the analysis, the broadband VIs were compared to the hyperspectral VIs to see if hyperspectral indices improve the prediction accuracy. All best narrowband *RVI* (*RVI\_opt*) and *PVI* (*PVI\_opt*) perform better than the corresponding broadband VIs. RMSE values of about 1  $m^2 m^{-2}$  or larger for regression models between broadband *RVI* and *LAI* (subsets *am*, *a*, and *m*) decrease to values as low as 0.5  $m^2 m^{-2}$  for the optimal narrowband *RVI*. The improvement of the narrowband models compared to the broadband models is not that distinct in the case of the *PVI*. Over all age classes *PVI\_opt* performs better than *RVI\_opt*; for subsets *mo*, *m*, and *o*, however, *RVI\_opt* shows lower RMSE values than *PVI\_opt*.

To sum up, it can be concluded that the hyperspectral data set contains more information relevant to the estimation of forest *LAI* than multispectral data. However, this does not always seem to be

valid: For instance, (24) came to the conclusion, that hyperspectral  $VIs$  derived from field spectral measurements were not better at estimating green crop area index (a variable related to  $LAI$ ) than traditional broadband  $VIs$ . For old stands of age 80 or more (subset o), relatively poor relationships were found particularly for the broadband  $VIs$ . Also other studies reported problems with old stands that have been ascribed to shadow effects and a relatively dark background in the nIR (5).

In the scatter plot between  $PVI_{opt}$  and  $LAI$  (Figure 3), even at high values of  $LAI$  no saturation is evident. A closer look reveals an outlier at position 4.1/-0.104. The corresponding forest stand of age 34 was identified in the image data. While the 1999 image showed no abnormality in reflectance, a striped pattern was detected in recently acquired HyMap data of 2003. From the spectral reflectance properties, the image pixels representing stripes could be identified as a mixture between tree crowns and forest litter. The striping pattern was caused by aisles that had been cut into the forest between the image acquisition and field measurements. Forest aisles allowed for the employment of harvesters in order to remove trees that had been exposed to game bite (personal communication of the responsible forest official, G. Womelsdorf, 25.02.2004).

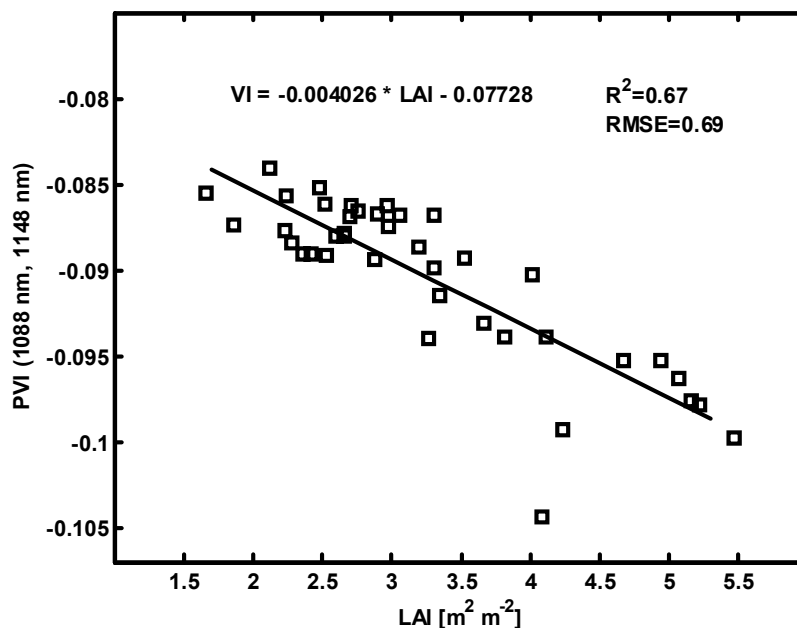


Figure 3: Linear regression between best narrowband PVI and LAI. Values of  $R^2$  and RMSE are cross-validated. When the outlier at position 4.1/-0.104 is removed, cross-validated  $R^2$  increases to 0.77 and RMSE decreases to  $0.54 \text{ m}^2 \text{ m}^{-2}$ .

## CONCLUSIONS

The following conclusions can be drawn from the research:

- Forest leaf area index ( $LAI$ ) and crown volume ( $VOL$ ) can be estimated with good accuracy from hyperspectral remote sensing data
- Orthogonal compared to ratio  $VIs$  are better suited to characterise forest  $LAI$  and  $VOL$
- Hyperspectral data contains more information relevant to the estimation of the forest stand variables  $LAI$  and  $VOL$  than multispectral data

## ACKNOWLEDGEMENTS

This research was for the most part financially supported by the German Research Community (DFG). Many thanks to Andreas Müller and Andrea Haushold (German Aerospace Center, DLR) for providing imaging spectrometer data. The authors would like to thank Patrick Hostert, Thomas Udelhoven, Wolfgang Mehl, Samuel Bärtsch and Sebastian Mader for their help with pre-

processing of the HyMap data. The authors are particularly grateful to Samuel Bärish for assistance in the field at Idarwald test site.

## REFERENCES

- 1 Treitz P M & P J Howarth, 1999. Hyperspectral remote sensing for estimating biophysical parameters of forest ecosystems. Progress in Physical Geography, 23: 359-390
- 2 Fassnacht K S; S T Gower, M D MacKenzie, E V Nordheim & T M Lillesand, 1997. Estimating the leaf area index of north central Wisconsin forests using the Landsat Thematic Mapper. Remote Sensing of Environment, 61: 229-245
- 3 Running S W; D L Peterson, M A Spanner & K B Teuber, 1986. Remote sensing of coniferous forest leaf area. Ecology, 67: 273-276
- 4 Badhwar G D; R B Macdonald, F G Hall & J G Carnes, 1986. Spectral characterization of biophysical characteristics in a boreal forest: Relationship between Thematic Mapper band reflectance and leaf area index for aspen. IEEE Transactions on Geoscience and Remote Sensing, GE-24: 322-326
- 5 Spanner M A; L A Pierce, D L Peterson & S W Running, 1990. Remote sensing of temperate coniferous forest leaf area index - The influence of canopy closure, understory vegetation and background reflectance. International Journal of Remote Sensing, 11: 95-111
- 6 Chen J M & J Cihlar, 1996. Retrieving leaf area index of boreal conifer forests using Landsat TM images. Remote Sensing of Environment, 55: 153-162
- 7 Franklin S E, M B Lavigne, M S Deuling, M A Wulder & E R Hunt Jr, 1997. Estimation of forest leaf area index using remote sensing and GIS data for modelling net primary production. International Journal of Remote Sensing, 18: 3459-3471
- 8 Brown L.; J M Chen, S G Leblanc & J Cihlar, 2000. A shortwave infrared modification to the simple ratio for LAI retrieval in boreal forests: An image and model analysis. Remote Sensing of Environment, 71: 16-25
- 9 Chen J M, G Pavlic, L Brown, J Cihlar, S G Leblanc, H P White, R J Hall, D R Peddle, D J King J A Trofymow, E Swift, J van der Sanden & P K E Pellikka, 2002. Derivation and validation of Canada-wide coarse-resolution leaf area index maps using high-resolution satellite imagery and ground measurements. Remote Sensing of Environment, 80: 165-184
- 10 Gong P, R Pu & J R Miller, 1995. Coniferous forest leaf area index estimation along the Oregon transect using Compact Airborne Spectrographic Imager data. Photogrammetric Engineering & Remote Sensing, 61: 1107-1117
- 11 Danson F M & S E Plummer, 1995. Red-edge response to forest leaf area index. International Journal of Remote Sensing, 16: 183-188
- 12 Lucas N S, P J Curran, S E Plummer & F M Danson, 2000. Estimating the stem carbon production of a coniferous forest using an ecosystem simulation model driven by the remotely sensed red edge. International Journal of Remote Sensing, 21: 619-631
- 13 Danson F M & E M Rollin, 1997. Information content of high spectral resolution reflectance data for forest canopies. In: Physical measurements and signatures in remote sensing, edited by G Guyot & P Thierry (Balkema, Rotterdam) 457-462
- 14 Hill J & W Mehl, 2003. Georadiometrische Aufbereitung multi- und hyperspektraler Daten zur Erzeugung langjähriger kalibrierter Zeitreihen. Photogrammetrie-Fernerkundung-Geoinformation, 1: 7-14

- 15 Schläpfer D; M E Schaepman & K I Itten, 1998: PARGE: Parametric Geocoding Based on GCP- Calibrated Auxiliary Data. In: SPIE International Symposium on Optical Science and Instrumentation (San Diego, CA) 334-344
- 16 Pearson R L & L D Miller, 1972. Remote mapping of standing crop biomass for estimation of the productivity of the short-grass prairie, Pawnee National Grasslands, Colorado. Proceedings of the 8th International Symposium on Remote Sensing of Environment, ERIM International: 1357-1381
- 17 Rouse J W, R H Haas & J A Schell, 1974. Monitoring the vernal advancement of retrogradation of natural vegetation. In: NASA/GSFC, Type III, Final Report (Greenbelt, MD, USA) 1-371
- 18 Richardson A J & C L Wiegand, 1977. Distinguishing vegetation from soil background information. Photogrammetric Engineering & Remote Sensing, 43: 1541-1552
- 19 Baret F; G Guyot & D J Major, 1989. Crop biomass evaluation using radiometric measurements. Photogrammetria (PRS), 43: 241-256
- 20 Christ E P & R C Cicone, 1984. A physically-based transformation of Thematic Mapper data - the TM Tasseled Cap. IEEE Transactions on Geoscience and Remote Sensing, GE-22: 256-263
- 21 Thenkabail P S; R B Smith & E De Paw, 2000. Hyperspectral vegetation indices and their relationships with agricultural crop characteristics. Remote Sensing of Environment, 71: 158-182
- 22 Vose J M; P M Dougherty, J N Long, F W Smith, H L Gholz & P J Curran, 1994. Factors influencing the amount and distribution of leaf area of pine stands. Ecological Bulletins, 43: 102-114
- 23 Boyd D S; T E Wicks & P J Curran, 2000. Use of middle infrared radiation to estimate the leaf area index of a boreal forest. Tree Physiology, 20: 755-760
- 24 Broge N H & J V Mortensen, 2002. Deriving green crop area index and canopy chlorophyll density of winter wheat from spectral reflectance data. Remote Sensing of Environment, 81: 45-57